Korean J. Chem. Eng., 36(9), 1432-1440 (2019)
DOI: 10.1007/s11814-019-0336-5

pISSN: 0256-1115
eISSN: 1975-7220

CO_2 capture and preparation of spindle-like $CaCO_3$ crystals for papermaking using calcium carbide residue waste via an atomizing approach

Liang Ma*,, Tingyu Yang**,***, Yu Wu**,***, Xiaoqing Yue**,***, Jinrong Yang**,***, Shuai Zhang**,***, Qiang Li**,***, and Jianbin Zhang*,**,***,†**

*Key Laboratory of Coal-based CO_2 Capture and Geological Storage, China University of Mining and Technology, Xuzhou, 221008, China
**College of Chemical Engineering, Inner Mongolia University of Technology, Hohhot 010051, China
***Inner Mongolia Engineering Research Center for CO_2 Capture and Utilization, Hohhot 010051, China
(*Received 25 January 2019 • accepted 7 July 2019*)

Abstract−Spindle-like $CaCO_3$ crystals with controllable sizes for papermaking were successfully prepared using CO_2 (8% CO_2/N_2 mixture gas) and calcium carbide residue (CCR) waste, a by-product of acetylene gas and polyvinyl chloride production, as the raw materials by an atomization method at room temperature. The influences of solution concentration, reaction temperature, and gas/liquid flow rate ratios on the properties of the $CaCO_3$ crystal were systematically investigated, and a possible atomization mechanism was proposed. The size of the as-prepared $CaCO_3$ crystal with pure calcite phase was turned from 4.71×4.02 μm to 1.82×1.12 μm by adjusting the reaction conditions. The application of the as-prepared $CaCO_3$ crystals from CCR waste as a filler for papermaking was explored. The R475 blue light whiteness of paper was increased from 77.3 to 80.6 with 11.4% $CaCO_3$ crystals.

Keywords: Calcium Carbide Residue (CCR), Spindle-like $CaCO_3$, Carbon Dioxide Capture, Atomization, Papermaking

INTRODUCTION

CO_2, a major greenhouse gas [1,2], has caused extreme climatic events worldwide [3,4], such as heat waves, droughts, and floods. According to the International Panel on Climate Change (IPCC), to stabilize the atmospheric CO_2 concentration, the global greenhouse gas (GHG) emissions must be reduced by as much as 80% by 2050 [5]. For this reason, carbon capture, utilization, and storage (CCUS) has been proposed for the greenhouse gas mitigation from flue gas streams in the concentration range of 4-15% [6-9]. The CO_2 mineral sequestration to $CaCO_3$ is an important CCUS approach with well-documented advantages, such as large capacity, no post-storage monitoring needed, and low energy consumption due to the exothermic chemical reaction, yet it is an expensive and low economic approach [10,11]. Reducing raw material cost and energy consumption are critical to make the CO_2 mineralization process more economically efficient.

Calcium carbide residue (CCR) is an industrial solid waste mainly discharged from ethylene and polyvinyl chloride (PVC) industrials as shown in Eq. (1) [12-14].

$$CaC_2+H_2O=C_2H_2+Ca(OH)_2 \quad (1)$$

CCR is a byproduct of the PVC industry with the annual yield of 5.6×10^7 t/y in the world [15]. Such CCR waste is usually stockpiled without being treated [3,16], which has caused serious environmental concerns, such as ground water pollution, occupation of land resources, and soil alkalization [17]. Therefore, treatment approaches and strategies are highly desired for reduction and harmlessness of CCR waste. Recently, some efforts have been reported for the utilization of CCR waste. Cao et al. [18] prepared an insulation material, xonotlite, via the dynamic hydrothermal synthesis using CCR waste as the calcareous material. Li et al. [19,20] found that the ultimate carbonation conversion of CCR waste is higher than limestone in the same number of cycles of calcium looping. Siddiqua et al. [21] demonstrated the application potentials of CCR waste for the preparation of soil-binders. Nevertheless, these reports failed to demonstrate the full application potentials of CCR waste. More new technologies are needed to prepare value-added materials with CCR waste to boost its utilization. CCR waste is mainly composed of $Ca(OH)_2$ (>80 wt%), along with some impurities, such as silicon, alumina, ferric, and magnesium. We reported previously the preparation of vaterite $CaCO_3$ micro-spheres by the hydrothermal reaction of CCR waste [22]. However, the process is of high cost with long reaction time. In the work, the preparation of $CaCO_3$ using CCR via atomization route has the advantages as follows: 1) No need for storage materials and high temperature, which can greatly reduce the cost. 2) The reaction was carried out through the direct contact of CO_2 and $Ca(OH)_2$, which can be operated continuously and reacted quickly. Therefore, mild conditions for the synthesis of $CaCO_3$ crystals from CCR waste is a feasible and worth developing approach to lowering the cost.

Precipitated calcium carbonate (PCC) has been applied to various fields, such as paper, paint, ink, food, plastics and rubber industries [23-25]. In particular, PCC is a common filler in the papermaking industry to improve the optical properties, smoothness, printability and sheet formation of paper [26-28]. Commercial $CaCO_3$ products have a special needle-like, cubic-like, sphere-like, or spin-

†To whom correspondence should be addressed.
E-mail: tadzhang@pku.edu.cn

dle-like morphology, among which the spindle-like $CaCO_3$ is widely used as the filler for papermaking with high bulk, air permeability and opacity [29]. PCC is usually produced by three methods, the carbonation process, the $Ca(OH)_2$-$NaCO_3$ process and the $CaCl_2$-$NaCO_3$ double salt decomposition process [28]. However, these methods require pure chemicals as the raw material, which inevitably leads to higher cost of production. In the papermaking industry, the feedstock cost usually accounts for more than 90% of the total production cost [30]. The substitution of costly raw materials with a low-cost feedstock has a promising prospect. Lime milk is made from calcined limestone, which consumes a large amount of energy and releases gaseous CO_2. The preparation of the value-added PCC using the solid CCR waste and the greenhouse gas CO_2 as the raw materials would not only produce economic values, but also reduce the greenhouse gas emission to realize the waste reutilization.

In the present work, spindle-like $CaCO_3$ crystals were successfully prepared via the reaction of CCR waste with 8 vol% CO_2 (typical flue gas component) by an atomization process. The application of the as-prepared $CaCO_3$ crystals as the filler for papermaking was explored. Our work with the emphasis on bridging the reutilization an industrial waste with enhanced commercial viability has provided a novel preparation method with low manufacturing cost and reduced CO_2 emission. The method shows the following significant advantages for the preparation of PCC. First, CCR and simulated flue gas are used as the raw materials, which provides a feasible way for the value-added utilization of CCR and CO_2. Second, no controlling agents are needed. Third, the preparation process can be carried out at room temperature and finished in a very short time. Fig. 1 shows the overall preparation process. Our study provides a reference for the efficacious utilization of CCR waste and opened an outstanding way to reduce CO_2 emission.

EXPERIMENTAL SECTION

1. Materials

CCR waste was sampled from an acetylene plant in the Zhungeer Qi Kaida Gas Manufacturing Co., Ltd., Inner Mongolia Autonomous Region, China, and dried at 100 °C for 6.0 h by the vacuum oven. $Ca(OH)_2$ was purchased from Sinopharm Chemical Reagent Co., Ltd. (purity >95%). 8 vol% CO_2 gas was used to provide carbon resource, which was purchased by Beijing North oxygen special gas company. Doubly distilled water with conductivity lower than 0.1 mS cm^{-1} (25 °C) was used. Paper pulp was purchased from ShengZe Paper Co., Ltd. for paper making. All other reagents used were of analytical grade.

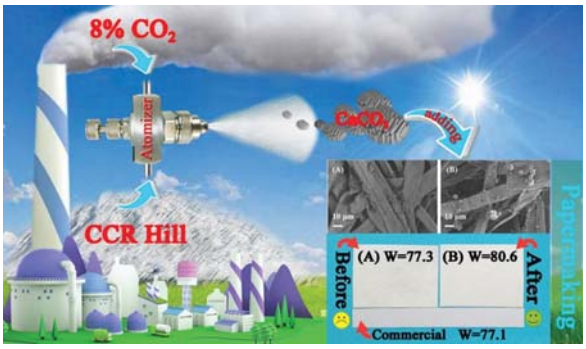

Fig. 1. Synthesis of spindle-like $CaCO_3$ by atomization way and effect of as-prepared $CaCO_3$ crystals on whiteness of paper making. The $CaCO_3$ crystals were synthesized by the CCR and simulated flue gas via an atomization. Then the as-obtained $CaCO_3$ was added into paper and the whiteness was investigated.

2. Characterization

Scanning electron microscopy (SEM, Quanta FEG 650, USA) was employed at an accelerating voltage of 20 kV. High magnification transmission electron (HR-TEM) and selected area electron diffraction micrographs (SAED, JEM-2100, Japan) were obtained at an accelerating voltage of 200 kV. X-ray powder diffraction (XRD) patterns of the samples were collected on a powder X-ray diffractometer Siemens D/max-RB) in the 2θ range of 5-80° at a scan speed of 10°/min using CuKα (λ=1.5418 Å) radiation. N_2 adsorption-desorption isotherms were recorded on a 3H-2000PS2 BET instrument at liquid nitrogen temperature (77.3 K). Surface area was determined using the Brunauer-Emmett-Teller (BET) method, and pore size distribution was calculated from the adsorption branch of the isotherms using the Barrett-Joyner-Halenda (BJH) model. Thermogravimetry-differential scanning calorimetry (TG-DSC, Entzsch-Sta 449, Germany) was conducted to measure the weight percentage of the samples at a heating rate of 5 °C min^{-1}. Furthermore, the relative percentage of each polymorph of the $CaCO_3$ precursors was calculated from their XRD patterns. The concentration of Ca^{2+} was measured by Bante 931 precision Ca^{2+} meter with accuracy of 0.1 mmol/L. The concentration of tail gas was monitored using an online gas intelligent CO_2 detector with the accuracy of ±3% F.S. Whiteness of as-made paper was measured by WSB-II meter with D65 light source. The chemical components of CCR were analyzed by X-ray fluorescence analyzer spectrometer (XRF, Rigaku ZSXPrimus II). Particle size distribution (PSD) data was obtained by laser particle size analyzer (measuring range: 0.1-1,000 μm, Bettersize2000E, China).

3. Preparation of $CaCO_3$

All $CaCO_3$ samples were prepared by the reaction of CCR waste and 8 vol% CO_2 with an atomizing nozzle. In a typical procedure, a saturated $Ca(OH)_2$ solution was placed in a thermostat tank for 20 min. Atomized droplets were formed by adjusting the pressure in the tank and collected with a container. The as-obtained suspension was vacuum filtered. The residue was washed with deionized water and dried in an oven at 120 °C for 2 h to afford the final $CaCO_3$ product.

4. Papermaking

Papermaking was conducted following a traditional papermaking process. Briefly, 10.0 g pulp was dispersed into 1.0 L deionized water and stirred vigorously at room temperature for 10 min. A $CaCO_3$ sample was added to the purple suspension to form an aqueous suspension of cellulose fiber pulp that was stirred for 10 min, filtered, and dried at 60 °C in air for 3.0 h to form the paper sample.

RESULTS AND DISCUSSION

1. Effect of Preparation Conditions

1-1. Effect of Solution Concentration

To develop a fast and feasible preparation method of $CaCO_3$

Table 1. As-prepared $CaCO_3$ crystals with different $Ca(OH)_2$ concentrations at gas flow of 43.9 L/min, liquid flow of 33.1 mL/min, and 20 °C

Samples No.	$Ca(OH)_2$ solution concentration	Average size (μm)
A	Saturation	4.71×4.02
B	90% Saturation	4.68×4.49
C	80% Saturation	4.89×4.25
D	70% Saturation	3.46×2.20
E	60% Saturation	2.89×2.06

crystals from CCR waste and to simply the experimental process, analytical-grade $Ca(OH)_2$ was used at first to optimize the atomization method. $CaCO_3$ crystals were prepared at the various $Ca(OH)_2$ concentrations, respectively, by the atomization method at 20 °C. Table 1 lists the preparation conditions and properties of each sample.

As shown in Fig. 2, spindle-like $CaCO_3$ crystals with the average sizes ranging from 4.71×4.02 μm to 2.89×2.06 μm were obtained. The sizes of samples A, B and C remained unchanged at first as $Ca(OH)_2$ concentration decreased (Table 1). Further decreasing $Ca(OH)_2$ concentration reduced the particle size from 3.46×2.20 μm to 2.89×2.06 μm. The Fig. S1 shows that the curves have two peaks, which are in the submicron range and the micron range, respectively. A noticeable shift can be observed that the maximum proportion decreased from 6.64 μm (5.48%) to 4.67 μm (6.8%). In addition, the peak of sample A is sharper, which indicates that the decrease of concentration is beneficial for the uniformity of $CaCO_3$ scale. Meanwhile, the crystal proportions of $CaCO_3$ were estimated with molar content (%) yield and intensity by Eqs. (2)-(4) in the XRD results (Fig. 3(I)).

$$X_A = \frac{3.157 \times I_A^{221}}{I_C^{104} + 3.157 \times I_A^{221} + 7.691 \times I_V^{110}} \quad (2)$$

$$X_C = \frac{I_C^{104} \times X_A}{3.175 \times I_A^{221}} \quad (3)$$

$$X_V = 1.0 - X_A - X_C \quad (4)$$

The characteristic peaks of aragonite were detected in sample A

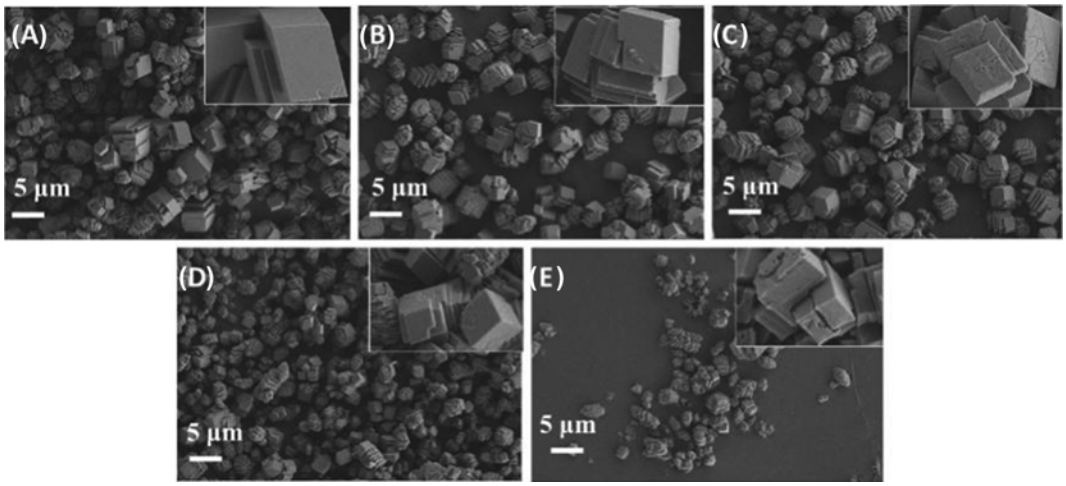

Fig. 2. SEM images of as-prepared $CaCO_3$ crystals. $Ca(OH)_2$ concentration of samples: (A) was saturation solution; (B), (C), (D) and (E) were 90%, 80%, 70% and 60% saturated $Ca(OH)_2$ aqueous solution at 20 °C.

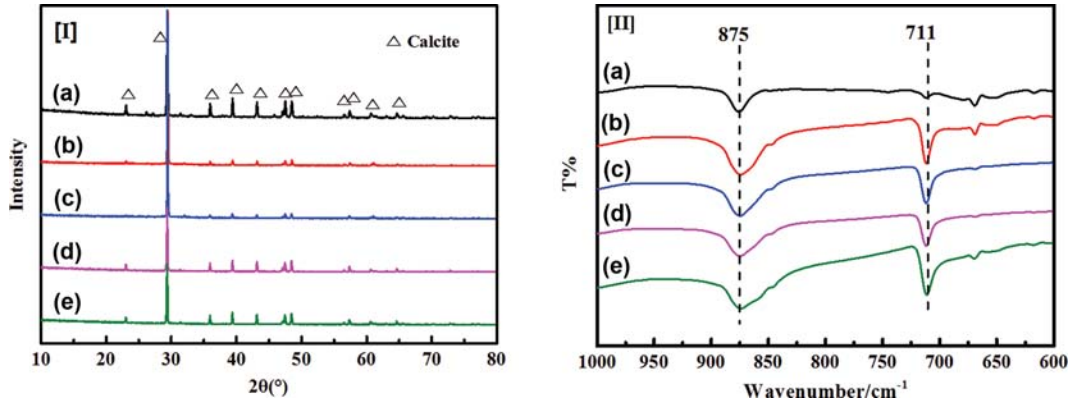

Fig. 3. XRD patterns (I) and FT-IR spectra (II) of as-prepared $CaCO_3$ crystals. The $Ca(OH)_2$ concentration of samples: (a) was saturation solution; (b), (c), (d) and (e) were 90%, 80%, 70% and 60% saturated $Ca(OH)_2$ aqueous solution at 20 °C.

in Table 1, but the intensity of the peaks was very weak. According to above calculation method, the ratio of aragonite is less than 1%. The estimated results showed that all samples were calcite structure, in which 2θ=23.00°, 29.35°, 35.88°, 39.31°, 43.05°, 47.45°, 48.43°, 57.23°, 60.53°, 64.50° and 66.4° correspond to (012), (104), (110), (113), (202), (018), (116), (122), (214), (300) and (423) planes of calcite (JCPD no. 05-0586), respectively [31-36]. Fig. 3(II) shows the FT-IR spectra of the $CaCO_3$ products. The absorption peaks at 875 (ν_2 mode of calcite) and 711 cm^{-1} (ν_4 mode of calcite) of samples A-E further confirm that they are calcites [37-39]. These suggest that the concentration of $Ca(OH)_2$ has no obvious effects on the morphology and crystal form of the as-prepared $CaCO_3$ crystals, but clearly affects the crystal size. The particle size of $CaCO_3$ crystal exhibited a decreasing trend with the decrease of $Ca(OH)_2$ concentration. It can be explained that the liquid, e.g., the $Ca(OH)_2$ solution, is impacted into tiny droplets by the high pressure gas, which greatly increases the mass transfer rate. The nucleation, growth, and self-assembly occurred in the tiny droplets. The limited raw material results smaller ultimate size of $CaCO_3$ crystals.

1-2. Effect of Temperature

The effect of solution temperature, an important parameter, was investigated at 10 °C, 20 °C, 40 °C and 60 °C, respectively. The preparation condition and properties of each samples are listed in Table 2.

As shown in Fig. 4 for the SEM images of the $CaCO_3$ crystals prepared at different temperatures, the morphology of $CaCO_3$ product was not significantly affected by the solution temperature. However, the particle size decreased from 3.53×2.66m to 2.36×2.06 μm and the size distribution became sharper as the solution temperature increased from 10 °C to 60 °C (Table 2, Fig. S3). The

Table 2. As-prepared $CaCO_3$ crystals with different temperatures of $Ca(OH)_2$ solutions at [$Ca(OH)_2$]=70% saturated solution, gas flow was 43.9 L/min, and liquid flow was 33.1 mL/min

Samples No.	Reaction temperature (°C)	Average size (μm)
A	10	3.53×2.66
B	20	3.46×2.20
C	40	3.15×2.17
D	60	2.36×2.06

XRD (Fig. 5(I)) and FT-IR (Fig. 5(II)) analyses indicate that all $CaCO_3$ products composed the pure calcite phase due to the fast nucleation [40]. Meanwhile, the solubility of $Ca(OH)_2$ decreased with the increase of temperature, which also contributed to the smaller particle sizes of the $CaCO_3$ crystals prepared at high temperatures.

1-.3 Effect of Gas and Liquid Flow Rate Ratio

The effects of the flow rates of gas and liquid on the $CaCO_3$ product were also investigated due to their effects on the atomization process. Fig. 6 shows the SEM images of the $CaCO_3$ crystals prepared at different.

Gas/liquid flow rate ratios had no significant effect on the morphology of $CaCO_3$ crystals was found. However the average particle size of the as-prepared $CaCO_3$ crystals decreased from 4.97×3.93 μm to 3.30×2.52 μm with the increase of gas flow (Table 3). The $CaCO_3$ crystals with the sizes as low as 1.82×1.12 μm were found due to the diminished liquid flow. However, no significant size change was observed as the liquid flow rate increased from

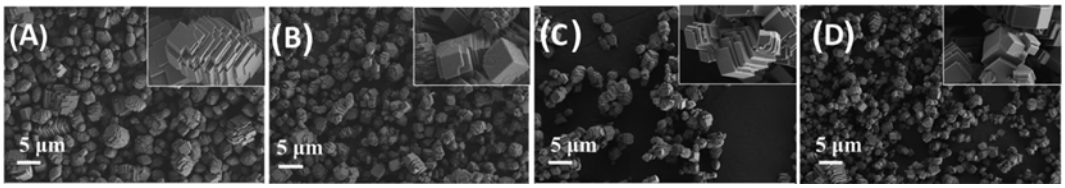

Fig. 4. SEM images of as-prepared $CaCO_3$ crystals for $Ca(OH)_2$ solutions at different temperatures: (A)=10 °C, (B)=10 °C, (C)=40 °C, and (D)=60 °C, respectively; [$Ca(OH)_2$]=70% saturated solution at 20 °C, gas flow was 43.9 L/min, and liquid flow was 33.1 mL/min.

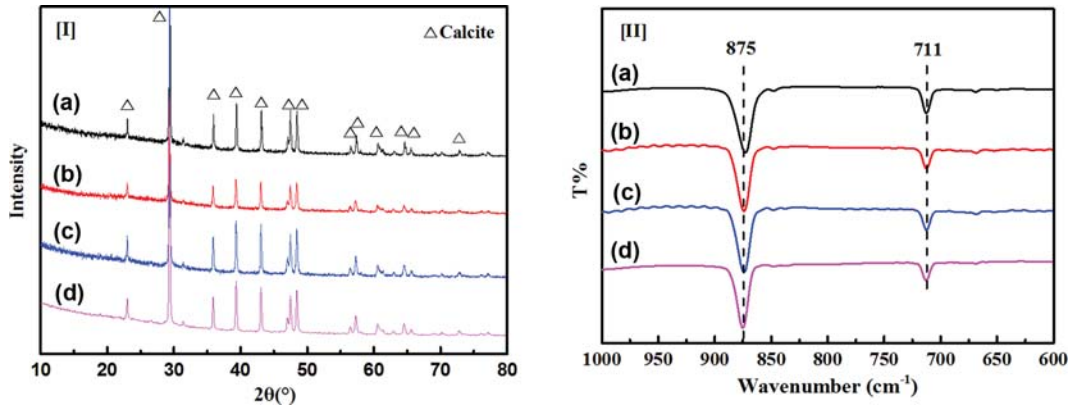

Fig. 5. XRD patterns (I) and FT-IR spectra (II) of as-obtained $CaCO_3$ crystals with different temperatures for $Ca(OH)_2$ solutions: (a)=10 °C, (b)=10 °C, (c)=40 °C, and (d)=60 °C, respectively; [$Ca(OH)_2$]=70% saturated solution at 20 °C, gas flow was 43.9 L/min, and liquid flow was 33.1 mL/min.

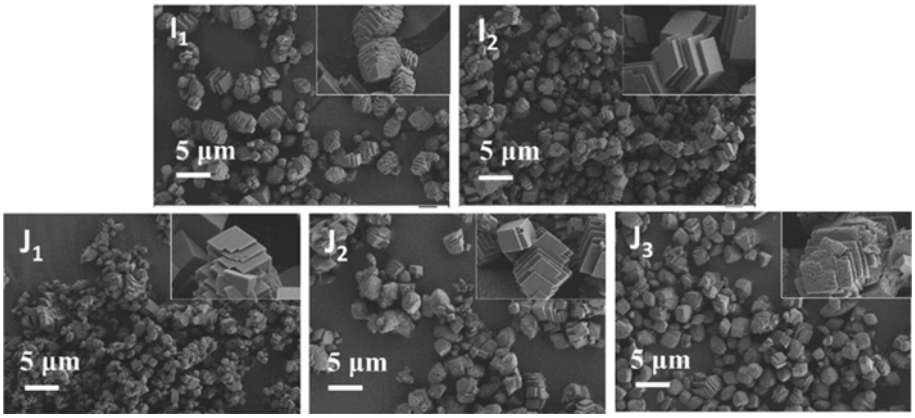

Fig. 6. The SEM images of as-obtained $CaCO_3$ with different gas flow and liquid flow: the gas flow of samples I_1, I_2, and J_{1-3} were 51.2 L/min, 37.9 L/min, and 43.9 L/min, respectively; the liquid flow of samples I_{1-2}, J_1, J_2 and J_3 were 33.1 mL/min, 20.0 mL/min, 39.3 mL/min and 53.3 mL/min, respectively; $[Ca(OH)_2]$=70% saturated solution at 20 °C.

Table 3. As-prepared $CaCO_3$ crystals with different gas flow and liquid flow with $[Ca(OH)_2]$=70% saturated solution at 20 °C

Samples No.	Gas flow (L/min)	Liquid flow (mL/min)	Average size (μm)
I_1	37.9	33.1	4.97×3.93
I_2	51.2	33.1	3.30×2.52
J_1	43.9	20.0	1.82×1.12
J_2	39.3	39.3	4.24×3.43
J_3	43.9	53.3	4.19×3.41

39.3 mL/min to 53.3 mL/min. These results indicate that the gas-liquid flow rate ratio can affect the particle size of $CaCO_3$ product and the particle size decreases with the increase of flow rate ratio. All samples were found to be the pure calcite structure (Fig. 7). The PSD spectra of the samples prepared at low gas and liquid flow rates were measured. The PSD peak became markedly broader with the decrease of gas and liquid flow rates, suggesting that the particle size of $CaCO_3$ crystals became less uniform.

The stable crystal form and morphology of the prepared $CaCO_3$ crystals are attributed to the fast nucleation and controlled thermodynamics [41,42]. The crystal size is affected by the conditions of atomization (the average size of atomized droplets), e.g., the gas-liquid flow rate ratio [11]. The tiny droplets are formed by the shear action of the gas on the liquid. Increasing the gas flow rate or decreasing the liquid flow rate results in stronger shear effect on the liquid, and thus smaller atomized droplets. The tiny droplets act as the microreactor to determine the final crystal size.

In all, the atomization conditions including solution concentration, solution temperature and gas/liquid flow rate ratios barely affect the morphology and crystal form of the $CaCO_3$ product, but are correlated with its particle size. The particle size decreases with the increase of temperature or/and gas/liquid flow rate ratio. The stable crystal form and morphology indicate the high tolerance of the process to the reactions conditions. In addition, the crystal size of product is tunable in the range from 4.97×3.93 μm to 1.82×1.12 μm.

2. Possible Crystallization Process of $CaCO_3$ Crystals

The carbonization of aqueous $Ca(OH)_2$ solution usually follows

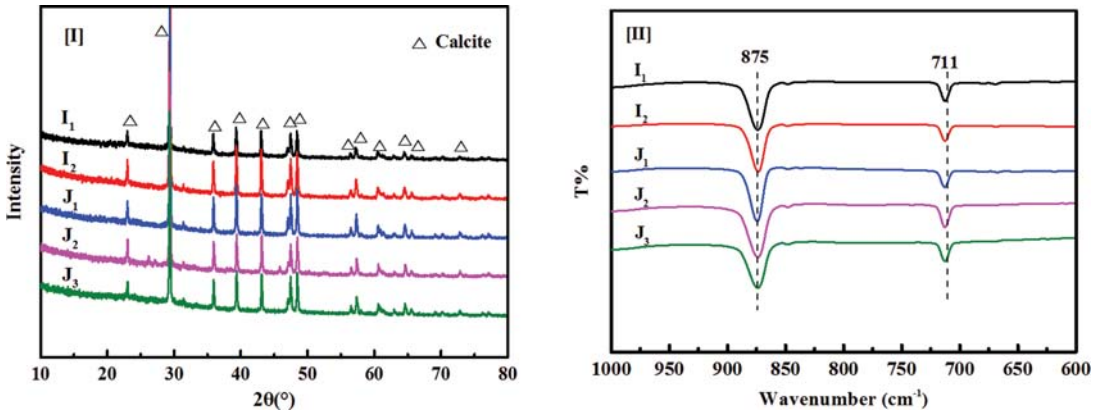

Fig. 7. XRD patterns (I) and FT-IR spectra (II) of as-prepared $CaCO_3$ crystals with different gas flow and liquid flow: the gas flow of samples I_1, I_2, and J_{1-3} were 51.2 L/min, 37.9 L/min, and 43.9 L/min, respectively; the liquid flow of samples I_{1-2}, J_1, J_2 and J_3 were 33.1 mL/min, 20.0 mL/min, 39.3 mL/min and 53.3 mL/min, respectively; and $[Ca(OH)_2]$=70% saturated solution at 20 °C.

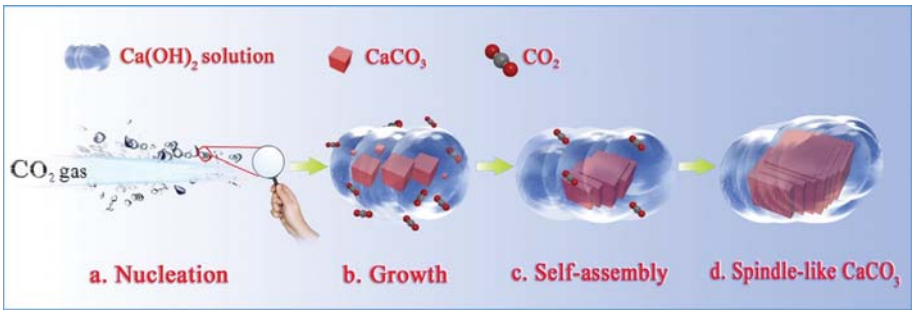

Fig. 8. Schematic diagram of the formation mechanism of spindle-like morphologies of $CaCO_3$ crystals.

the steps below [43,44].

$$Ca(OH)_{2(s)} \rightleftharpoons Ca^{2+}_{(aq)} + OH^-_{(aq)} \quad (5)$$

$$CO_{2(g)} \rightleftharpoons CO_{2(aq)} \quad (6)$$

$$CO_{2(aq)} + OH^-_{(aq)} \rightleftharpoons HCO^-_{3\,(aq)} \quad (7)$$

$$HCO^-_{3\,(aq)} + OH^-_{(aq)} \rightleftharpoons H_2O + CO^{2-}_{3\,(aq)} \quad (8)$$

$$Ca^{2+} + CO^{2-}_3 \rightleftharpoons CaCO_3 \quad (9)$$

In the present work, $Ca(OH)_2$ was completely ionized to Ca^{2+} and OH^-, which provided sufficient OH^- to keep an alkaline environment for the CO_2 absorption. Meanwhile, Ca^{2+} reacted with CO_3^{2-} to form $CaCO_3$ in a large number of tiny droplets ($Ca(OH)_2$ solution) formed under the impact of high-speed gas flow (8% CO_2). The nucleation, growth and self-assembly of $CaCO_3$ crystals then occurred in the droplets. Therefore, the size of atomized droplets exhibited a prominent effect on the size of as-prepared crystals. Fig. 8 shows a typical crystallization process of $CaCO_3$. First, $Ca(OH)_2$ solution is substantially dispersed into tiny droplets due to the strong shear force, and $CaCO_3$ crystal nuclei are formed immediately (Fig. 8(a)). The as-formed droplets are irregular spheres that collide and merge with each other under the action of a disturbing airflow. The tiny droplets are then ejected under the effect of the airflow and the nuclei begin to grow (Fig. 8(b)) and self-assemble under the van der Waals forces [45] to eventually form the spindle-like $CaCO_3$ crystals with the consumption of Ca^{2+} and CO_2 (Fig. 8(c)).

3. As-obtained $CaCO_3$ Crystals from CCR Waste

The results presented above were obtained using $Ca(OH)_2$ as the raw material to optimize the atomization conditions for preparing spindle-like $CaCO_3$ crystals. Under the optimal conditions, the preparation of $CaCO_3$ crystals from the CCR waste was then explored.

XRF analysis suggests that CCR is mainly composed of $Ca(OH)_2$ in the form of CaO with the content of ~75%. There also are 8% C, 4% SiO_2, 2% Al_2O_3, 0.5% Fe_2O_3, 0.2% MgO, 0.03% Na_2O and 10.27% impurities in the CCR waste. The broad XRF peak suggests that the raw material is heterogeneous (Fig. S5). The as-prepared $CaCO_3$ sample K exhibited the same morphology as the sample D with the average particle size of 4.48×3.95 μm (Fig. 9).

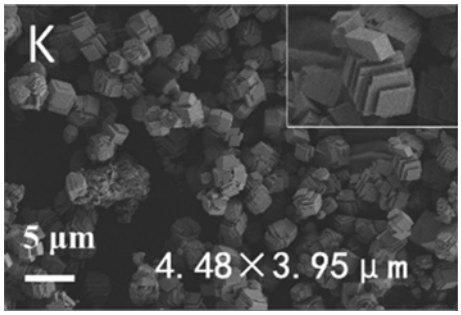

Fig. 9. SEM image of sample K prepared from saturated CCR solution at 20 °C via atomization method.

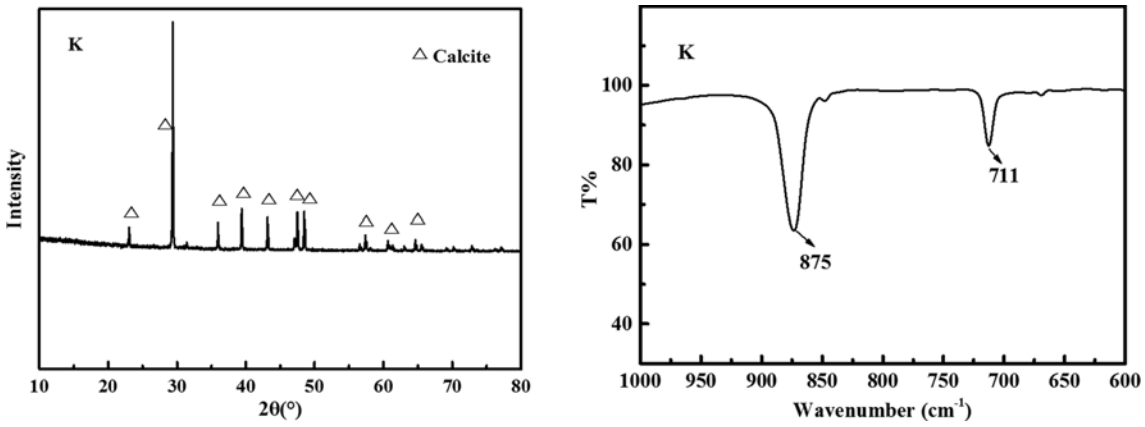

Fig. 10. XRD patterns (I) and FT-IR spectra (II) of $CaCO_3$ crystals prepared from saturated CCR solution at 20 °C via atomization method.

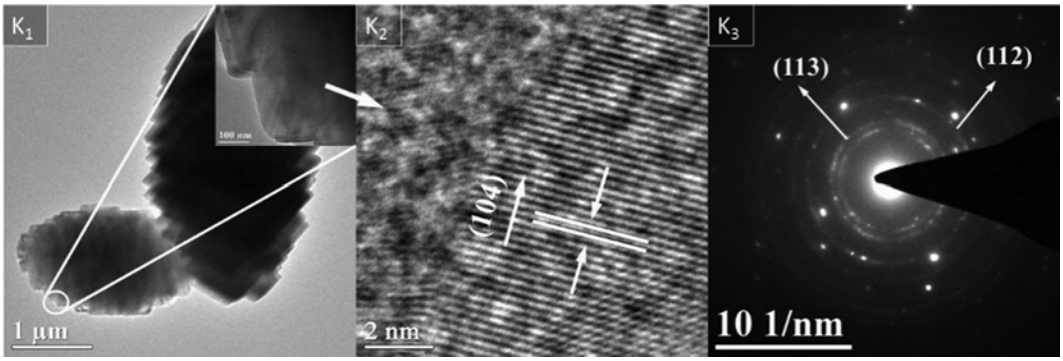

Fig. 11. HR-TEM images and SAED patterns of the as-prepared $CaCO_3$ crystals with 20 °C saturated CCR solutions and 8% CO_2. The gas and liquid flow rates are 43.9 L/min and 33.1 mL/min, respectively.

The XRD and FT-IR analyses suggest that they are pure calcite structure, and thus the atomization method is suitable for preparing $CaCO_3$ with CCR waste (Fig. 10). The Ca^{2+} concentration in the filtrate and the tail gas was measured to be 5.19 mmol/L and 7.62 vol%, respectively, suggesting that the atomization could effectively remove Ca^{2+} from the CCR waste.

4. Properties of $CaCO_3$ Crystals

To understand their structure, the $CaCO_3$ crystals prepared with CRR waste were characterized by HR-TEM, TGA-DSC, and N_2 adsorption-desorption isotherm.

4-1. HR-TEM

Fig. 11 shows the HR-TEM images of the $CaCO_3$ crystals prepared with CRR waste by the atomization method, and the locally enlarged images are mosaic in the upper right corner. It is clear that the spindle-like $CaCO_3$ crystals are composed of a large number of cubic micro-particles. The lattice spacing was measured to be 0.30 nm, that could be assigned to the (104) plane (Fig. 11 K_2) [46]. The rightmost column of the graph is the corresponding SAED pattern with the crystal planes labeled.

4-2. TGA-DSC

The TGA-DSC curves of the as-prepared $CaCO_3$ crystals were measured at a heating rate of 5 °C/min and two weight losses were observed (Fig. 12). The first weight loss of ~6.4% in the temperature range of 50-675 °C was mainly due to the losses of the adsorbed water and crystalline water. The higher weight loss at 675-775 °C was attributed to the decomposition of $CaCO_3$ [47-49].

4-3. N_2 Adsorption-Desorption Isotherm

Sample K exhibited a narrow pore size distribution centered at 3.71 nm (Fig. 13). Based on its pore size distribution curve, the specific surface area of sample K was calculated to be 2.56 m^2/g (Fig. 13). Its total pore volume and the average pore diameter were calculated to be 0.0272 cm^3/g and 41.0 nm, respectively.

5. Whitening Effects of the As-prepared Spindle-like $CaCO_3$ Crystals on Papermaking

In the papermaking industry, spindle-like $CaCO_3$ crystals are widely used due to their bridging effect [50], especially the whitening effect. In the present study, whiteness of the paper prepared using the as-prepared spindle-like $CaCO_3$ crystals as the filler was investigated.

$CaCO_3$ crystals were observed on the surface and intersecting crevice of fibers in the paper prepared using $CaCO_3$ crystals as the filler (Fig. 14). The paper sample A prepared by the conventional process exhibited two diffraction peaks at 15.6° and 22.5° that were respectively due to the (101) and (002) crystal planes of cellulose I in the paper [51]. New diffraction peaks corresponding to the

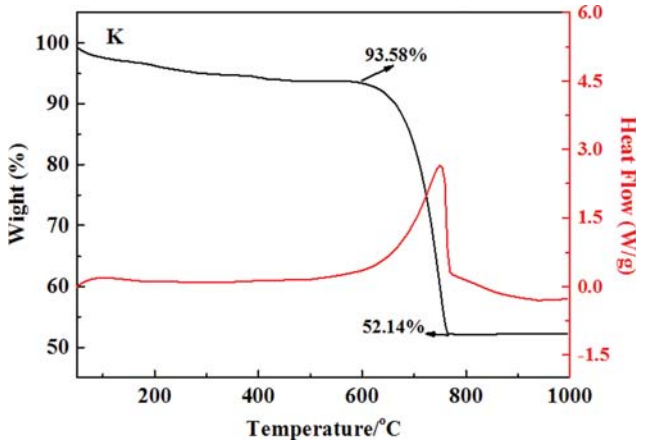

Fig. 12. TGA and DSC plots of as-prepared $CaCO_3$ crystals from CCR waste.

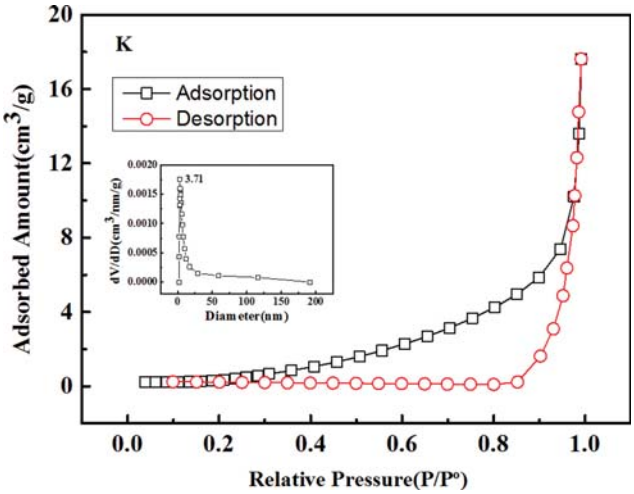

Fig. 13. N_2 adsorption-desorption isotherm of as-prepared $CaCO_3$ crystals from CCR waste.

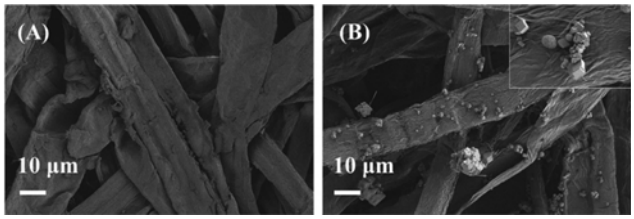

Fig. 14. SEM images of paper sample prepared: (A) was non $CaCO_3$ added paper, and (B) was $CaCO_3$ added paper.

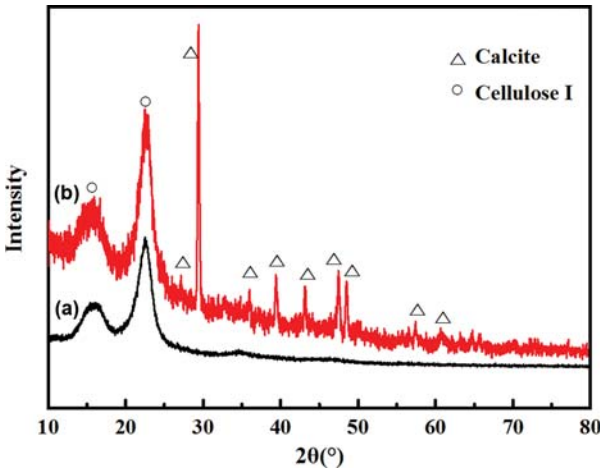

Fig. 15. The XRD curves of paper sample prepared: A was non $CaCO_3$ added paper, and B was $CaCO_3$ added paper.

$CaCO_3$ crystals of calcite structure were found in paper sample B that was prepared using 11.4% $CaCO_3$ crystals as the filler. It is clear that paper B is much whiter than paper A (Fig. 16). The R475 blue light whiteness of paper A was measured to be 77.3, similar to that of commercially available papers. Paper B exhibited the R475 blue light whiteness of 80.6, suggesting that its whiteness was significantly enhanced.

The $CaCO_3$ content in paper A and B was determined by TGA (Fig. 17). The TGA-DSC curve of paper A consists of a weight loss of ~3.8% at 50-300 °C due to the loss of the adsorbed water and a

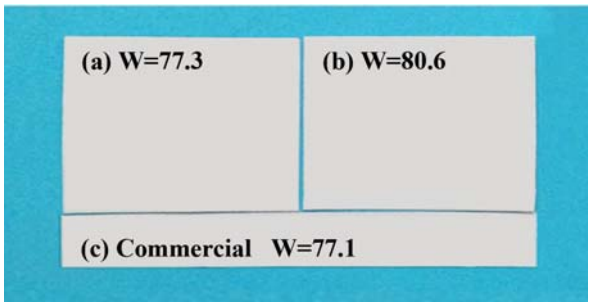

Fig. 16. The effect of $CaCO_3$ addition on the whiteness of paper: (a) was non $CaCO_3$ added paper, (b) was $CaCO_3$ added paper and (c) was purchased paper.

higher weight loss of ~65.9% at 350-400 °C with an obvious exothermic peak due to the decomposition of cellulose [52,53]. Paper B showed a weight loss of 5% at 650-700 °C, which was attributed to the decomposition of $CaCO_3$ into CaO and CO_2.

CONCLUSION

To simplify the experimental process, $CaCO_3$ crystals were first prepared with $Ca(OH)_2$ and 8% CO_2 by an atomization method to optimize the preparation conditions. The results suggest that the size of $CaCO_3$ crystals decreases with the increase of temperature and gas/liquid flow rate ratio, and the decrease of Ca^{2+} concentration, yet the crystal form and morphology are not significantly affected by the variation of reaction conditions. Based on these results, spindle-like $CaCO_3$ crystals, a similar morphology, were successfully prepared using CCR waste and 8% CO_2 as the raw materials by this green and economic atomization method. The application of the as-prepared $CaCO_3$ crystals from CCR waste as a filler for papermaking was explored. It was found that the whiteness of as-prepared paper was increased from 77.3 to 80.6 with 11.4% $CaCO_3$ crystals.

ACKNOWLEDGEMENTS

This work was supported by the National Natural Science Foundation of China (21666027), the Program for Grassland Excellent

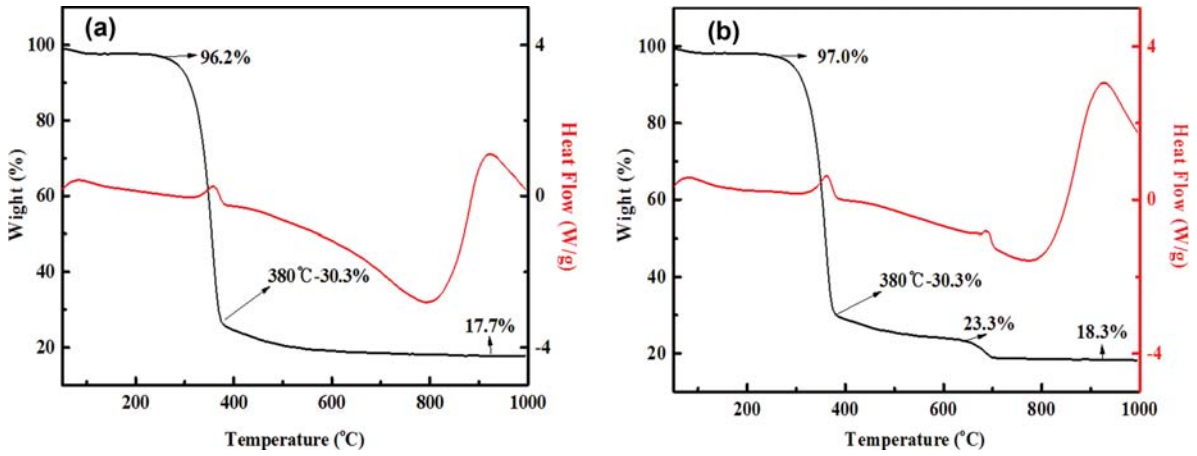

Fig. 17. TGA-DSC curves of paper sample prepared: (a) was non $CaCO_3$ added paper, and (b) was $CaCO_3$ added paper.

Talents of Inner Mongolia Autonomous Region, the Natural Science Foundation of Inner Mongolia Autonomous Region (2016JQ02), Key Laboratory of Coal-based CO_2 Capture and Geological Storage (Jiangsu Province, China University of Mining and Technology, 2016A06), the Inner Mongolia Science and Technology Key Projects, and training plan of academic backbone in youth of Inner Mongolia University of Technology.

SUPPORTING INFORMATION

Additional information as noted in the text. This information is available via the Internet at http://www.springer.com/chemistry/journal/11814.

REFERENCES

1. R. Monastersky, *Nature*, **497**, 13 (2013).
2. O. Buyukcakir, S. Je, S. Talapaneni, D. Kim and A. Coskun, *ACS Appl. Mater. Inter.*, **9**, 7209 (2017).
3. P. Cox, R. Betts, C. Jones, S. Spall and I. Totterdell, *Nature*, **408**, 184 (2000).
4. J. Lee, H. Lee, S. Lim, B. Kim and J. Choi, *J. Am. Chem. Soc.*, **137**, 7210 (2015).
5. L. S. Olabisi, P. B. Reich, K. A. Johnson, A. R. Kapuscinski, S. Suh and E. J. Wilson, *Environ. Sci. Technol.*, **43**, 1696 (2009).
6. Z. Yuan, M. Eden and R. Gani, *Ind. Eng. Chem. Res.*, **55**, 3383 (2016).
7. G. Alonso, D. Bahamon, F. Keshavarz, X. Gimenez, P. Gamallo and R. Sayos, *J. Phys. Chem. C*, **122**, 3945 (2018).
8. R. Zou, A. I. Abdel-Fattah, H. Xu, Y. Zhao and D. D. Hickmott, *CrystEngComm*, **12**, 1337 (2010).
9. J. A. Thote, R. V. Chatti, K. S. Iyer, V. Kumar, A. N. Valechha, N. K. Labhsetwar, R. B. Biniwale, M. K. N. Yenkie and S. S. Rayalu, *J. Environ. Sci.*, **24**, 1979 (2012).
10. J. K. Stolaroff, G. V. Lowry and D. W. Keith, *Energy Convers. Manage.*, **46**, 687 (2005).
11. W. J. J. Huijgen, *WurWageningen Ur*, **3**, 13 (2007).
12. K. Amnadnua, W. Tangchirapatand and C. Jaturapitakku, *Mater. Des.*, **51**, 894 (2013).
13. S. Dueramae, W. Tangchirapat and C. Jaturapitakkul, *Adv. Powder Technol.*, **29**, 672 (2018).
14. F. Cardoso, H. Fernandes, R. Pileggi, M. Cincotto, V. John, H. Fernandes, R. Pileggi, M. Cincotto and V. John, *Powder Technol.*, **195**, 143 (2009).
15. D. Zhang, S. Li, W. Song and W. Lin, *Energy Source Part A.*, **38**, 577 (2016).
16. C. Rattanashotinunt, P. Thairit, W. Tangchirapat and C. Jaturapitakkul, *Mater. Des.*, **46**, 106 (2013).
17. J. Cheng, J. Zhou, J. Liu, X. Cao and K. Cen, *Energy Fuel*, **23**, 2506 (2009).
18. J. Cao, F. Liu, Q. Lin and Y. Zhang, *Prog. Nat. Sci.*, **18**, 1147 (2008).
19. Y. Li, M. Su, X. Xie, S. Wu and C. Liu, *Appl. Energy*, **145**, 60 (2015).
20. Y. Li, R. Sun, C. Liu, H. Liu and C. Lu, *Int. J. Greenh. Gas Con.*, **9**, 117 (2012).
21. N. CesarConsoli, R. BeckSaldanha, J. CorrêaMallmann, T. Paula and B. ZakhariaHoch, *Constr. Build. Mater.*, **157**, 65 (2017).
22. B. Guo, T. Zhao, F. Sha, Z F. hang, Q. Li, J. Zhao and J. Zhang, *J. CO_2 Util.*, **18**, 23 (2017).
23. S. Kirboga and M. Oner, *CrystEngComm*, **15**, 3678 (2013).
24. M. Vinoba, M. Bhagiyalakshmi, G A. race, C D. hu, S. Nam, Y Y. oon, S. Yoon and S. Jeong, *Langmuir*, **29**, 15655 (2013).
25. H. Wang, V. Alfredsson, J. Tropsch, R. Ettl and T. Nylander, *ACS Appl. Mater. Inter.*, **5** 4035 (2013).
26. D. Chen and T. G. M. V. D. Ven, *Colloids Surf., A: Physicochem. Eng. Asp.*, **504**, 11 (2016).
27. T. Nypelo, M. Osterberg and J. Laine, *ACS Appl. Mater. Inter.*, **3**, 3725 (2011).
28. A. Said, H. Mattila, M. Järvinen and R. Zevenhoven, *Appl. Energy*, **112**, 765 (2013).
29. J. Wang, P. Wei, P. Liu and W. Sun, *BioResources*, **7**, 5894 (2012).
30. A. M. Chapman, C. Keyworth, M. R. Kember, A. J. J. Lennox and C. K. Williams, *ACS Catal.*, **5**, 1581 (2015).
31. S. Xu, Z. Ye and P. Wu, *ACS Sustain. Chem. Eng.*, **3**, 1810 (2015).
32. H. Nebel, M. Neumann, C. Mayer and M. Epple, *Inorg. Chem.*, **47**, 7874 (2008).
33. S. Kirbogan, M. Oner and E. Akyol, *J. Cryst. Growth*, **401**, 266 (2014).
34. S. Gopi, V. Subramanian and K. Palanisamy, *Ind. Eng. Chem. Res.*, **54**, 3618 (2015).
35. A. Lopez-Marzo and J. Merkoci, *J. Mater. Chem.*, **22**, 15326 (2012).
36. J. Wu and R. J. Zeng, *Cryst. Growth Des.*, **17**, 1854 (2017).
37. J. H. Xiang, H. Q. Cao, J. H. A. Warner and A. R. Watt, *Cryst. Growth Des.*, **8**, 4583 (2008).
38. L. Zheng, Y. L. Hu, Y. J. Ma, Y. Zhou, F. Nie, X. Liu and C. H. Pei, *J. Cryst. Growth*, **361**, 217 (2012).
39. Z. Zheng, B. Huang, H. Ma, Z X. hang, M. Liu, Z. Liu, K. Wong and W. Lau, *Cryst. Growth Des.*, **7**, 1912 (2007).
40. F. Sha, N. Zhu, Y. Bai, Q. Li, B. Guo, T. Zhao, F. Zhang and J. Zhang, *ACS Sustain. Chem. Eng.*, **4**, 3032 (2016).
41. X. Geng, L. Liu, J. Jiang and S. Yu, *Cryst. Growth Des.*, **10**, 3448 (2010).
42. S. Dickinson and K. Mcgrath, *J. Mater. Chem.*, **13**, 928 (2003).
43. S. J. Han, M. Yoo, D. W. Kim and J. H. Wee, *Energy Fuel*, **25**, 3825 (2011).
44. J. Yang, S. Shih, C. Wu and C. Y. Tai, *Powder Technol.*, **202**, 101 (2010).
45. Z. Zhang, D. Gao, H. Zhao, C. Xie, G. Guan, D. Wang and S. Yu, *J. Phys. Chem. B*, **110**, 8613 (2006).
46. L. Liu, D. He, G. Wang and S. Yu, *Langmuir*, **27**, 7199 (2011).
47. J. W. Butler, C. J. Lim and J. R. Grace, *Fuel*, **127**, 78 (2014).
48. L. Ma, B. Zhao, H. Shi, F. Sha, C. Liu, H. Du and J. B. Zhang, *CrystEngComm.*, **19**, 7132 (2017).
49. A. Biasin, C. U. Segre and M. Strumendo, *Cryst. Growth Des.*, **15**, 5188 (2015).
50. R. Gaudreault, N. Cesare, T. Ven and D. Weitz, *Ind. Eng. Chem. Res.*, **54**, 6243 (2015).
51. F. Boissou, A. Mühlbauer, K. D. O. Vigier, L. Leclercq, W. Kunz, S. Marinkovic, B. Estrine, V. Nardello-Rataj and F. Jérôme, *Green Chem.*, **16**, 2463 (2014).
52. Z. Wang, Y. Zhang, F. Jiang, H. Fang and Z. Wang, *Polym. Chem.*, **5**, 3379 (2014).
53. M. Semsarilar, J. Tom, V. Ladmiral and S. Perrier, *Polym. Chem.*, **3**, 3266 (2012).

Supporting Information

CO_2 capture and preparation of spindle-like $CaCO_3$ crystals for papermaking using calcium carbide residue waste via an atomizing approach

Liang Ma[*,], Tingyu Yang[**,***], Yu Wu[**,***], Xiaoqing Yue[**,***], Jinrong Yang[**,***], Shuai Zhang[**,***], Qiang Li[**,***], and Jianbin Zhang[*,**,***,†]**

*Key Laboratory of Coal-based CO_2 Capture and Geological Storage, China University of Mining and Technology, Xuzhou, 221008, China

**College of Chemical Engineering, Inner Mongolia University of Technology, Hohhot 010051, China

***Inner Mongolia Engineering Research Center for CO_2 Capture and Utilization, Hohhot 010051, China

(*Received 25 January 2019 • accepted 7 July 2019*)

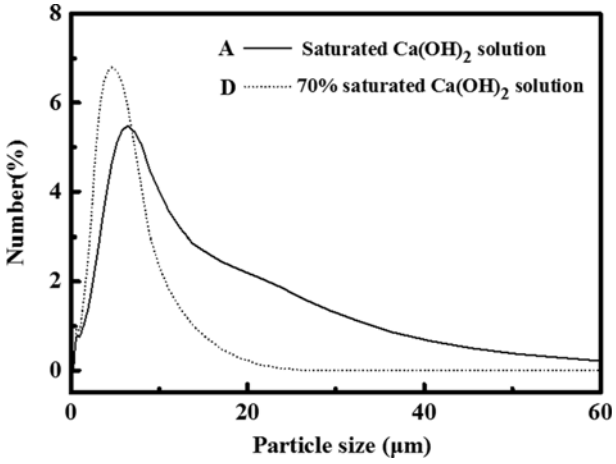

Fig. S1. PSD patterns of as-prepared $CaCO_3$ crystals with different $Ca(OH)_2$ concentrations at gas flow of 43.9 L/min, liquid flow of 33.1 mL/min, and 20 °C.

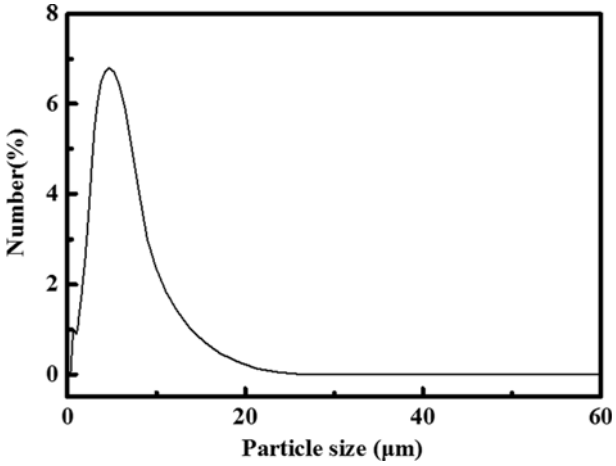

Fig. S2. PSD pattern of as-prepared $CaCO_3$ crystals with 70% saturated $Ca(OH)_2$ concentrations at gas flow of 43.9 L/min, liquid flow of 33.1 mL/min, and 20 °C.

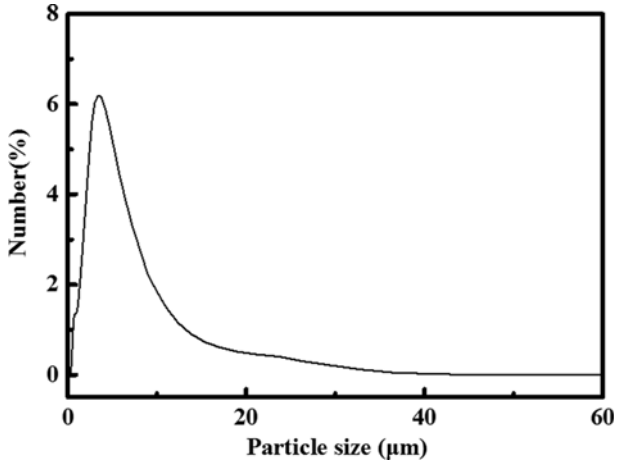

Fig. S3. PSD pattern of as-prepared $CaCO_3$ crystals at the temperatures of 60 °C with $[Ca(OH)_2]$=70% saturated solution, gas flow was 43.9 L/min, and liquid flow was 33.1 mL/min.

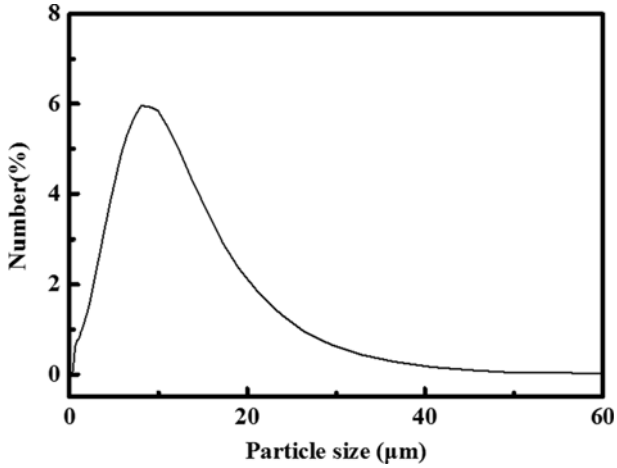

Fig. S4. PSD pattern of as-prepared $CaCO_3$ crystals at the temperatures of 60 °C with $[Ca(OH)_2]$=70% saturated solution, gas flow was 37.9 L/min, and liquid flow was 53.3 mL/min.

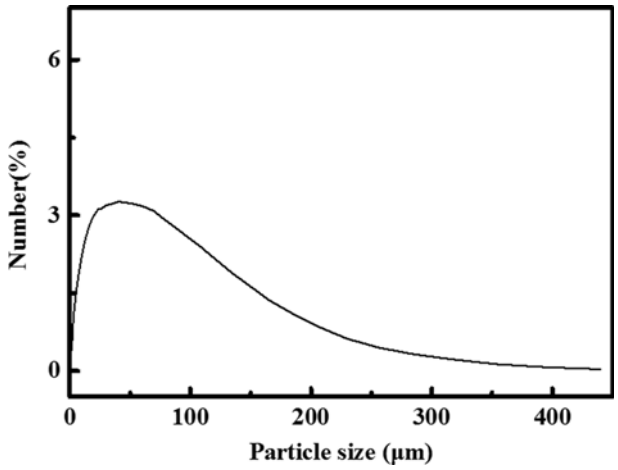

Fig. S5. PSD pattern of CCR raw materials.